Polymer Chemistry

ROYAL SOCIETY OF CHEMISTRY

PAPER

View Article Online
View Journal

Cite this: DOI: 10.1039/d6py00373g

Temperable dynamic polymeric glasses as tunable and rebondable adhesives

Kexin Li,[a] Nicholas R. Boynton, [b] Joseph M. Dennis,[c] Simon A. Fawcett [b] and Stuart J. Rowan *[a,b]

Dynamic covalent polymer networks offer a promising strategy for developing recyclable and stimuli-responsive adhesives. However, direct modulation of adhesive strength remains challenging. The focus of this work is on designing glassy dynamic networks that are capable of being tempered to access a range of mechanical properties dictated by the tempering temperature (T_t) they are exposed to and exploring their ability as glassy adhesives. To this end a series of thia-Michael (tM) dynamic networks constructed from rigid benzalcyanoacetate (BCA) and benzalcyanoacetamide (BCAm) ditopic acceptors crosslinked with a tetrathiol were prepared. The electronic nature of the β-phenyl moieties on the BCA and BCAm acceptors controls the amount of thia-Michael adduct formed resulting in materials with a range of crosslink densities and glass transition temperatures (T_g). All the resulting dynamic networks exhibit dynamic reaction-induced phase separation (DRIPS) to yield robust two-phase materials. Tempering within the thermal window between T_g and the upper transition temperature (T_{UT}) enables systematic tuning of network adduct fraction and crosslink density, leading to controllable changes in storage modulus, fracture toughness, and glass transition temperature within the same material. These thermomechanical variations translate directly to tunable adhesive performance, with lap shear strengths adjustable across multiple substrates, including aluminum and polyetherimide. The ability to modulate adhesive shear strength through thermal tempering highlights the potential of thia-Michael dynamic glasses as tunable structural adhesives for adaptive materials applications.

Received 15th April 2026,
Accepted 1st June 2026

DOI: 10.1039/d6py00373g

rsc.li/polymers

Introduction

Polymeric glasses are amorphous polymers with a glass transition temperature (T_g) above room temperature. They are exemplified by high stiffness and strength and generally exhibit low extensibility. One important application of such glasses is as structural adhesives for uses in a variety of fields, including construction, marine, aerospace, and electronics, where permanent, one-way bonding imparts high adhesive strength.[1,2] However, this irreversibility hinders reshaping or reprocessing of the adhesive network after curing. To address this limitation, prior studies have introduced intermolecular interactions, coordination bonds, or composite architectures to enable recyclable and self-healing glassy adhesives with robust mechanical properties.[3,4] In addition, debondable adhesives have been realized by "switching off" adhesion strength on-demand through external stimuli—including temperature, light, electric or magnetic fields, and chemical triggers—that alter interfacial adhesion, stiffness, contact area, or suction pressure.[5–9]

Among the strategies for accessing debondable adhesives, embedding dynamic covalent chemistries into a polymeric network has gained some attention over the past decade.[10,11] Dynamic covalent chemistry is reversible chemistry whose equilibrium/exchange rate can be tuned by external stimuli such as light, heat, or pH and their incorporation into a polymer networks yields dynamic covalent networks (DCNs) that are able to respond to an external stimulus resulting in a change in the physical structure or state of the network.[12] The dynamic covalent bonds in DCNs enable structural rearrangement within the network that brings new behavior to the resulting polymer (recyclability, self-healing, shape memory, and improvement in toughness).[13,14] A range of dynamic covalent bonds, including esters,[15–18] disulfide,[19–21] borate esters,[22–24] and Diels–Alder adducts,[25,26] have been incorporated into networks to yield dynamic covalent glassy adhesives, which can undergo crosslink exchange triggered by various stimuli to access rebondable and recyclable adhesives. Despite these advances, precise control over adhesive strength through

[a]Department of Chemistry, The University of Chicago, Chicago, Illinois, 60637, USA. E-mail: stuartrowan@uchicago.edu
[b]Pritzker School of Molecular Engineering, The University of Chicago, Chicago, Illinois 60637, USA
[c]Polymers Branch, U.S. Army DEVCOM Army Research Laboratory, Aberdeen Proving Ground, Maryland, 21005, USA

direct modulation of adhesive forces remains rare, yet such capability would open new opportunities in robotics, biomedical devices, and adaptive material systems.

One versatile class of dynamic covalent chemistry that has shown impressive tunability is the thia-Michael (tM) reaction, which is the addition of a thiol across an α,β-unsaturated carbonyl compound,[27–29] and a wide variety of dynamic networks have been investigated using the thia-Michael bond.[30–33] A subset of such chemistry is the addition of thiols to the benzalcyanoacetate (BCA) and benzalcyanoacetamide (BCAm) Michael acceptors, which have been shown to yield room-temperature, catalyst-free dynamic tM bonds with equilibrium constants (K_{eq}) that can be modulated over nearly three orders of magnitude, ~10 to 1000 M^{-1} for the BCA acceptors and *ca.* 100–9500 M^{-1} for the BCAm acceptors, by varying the electronic character of the β-phenyl moiety (Fig. 1a and b).[34–36]

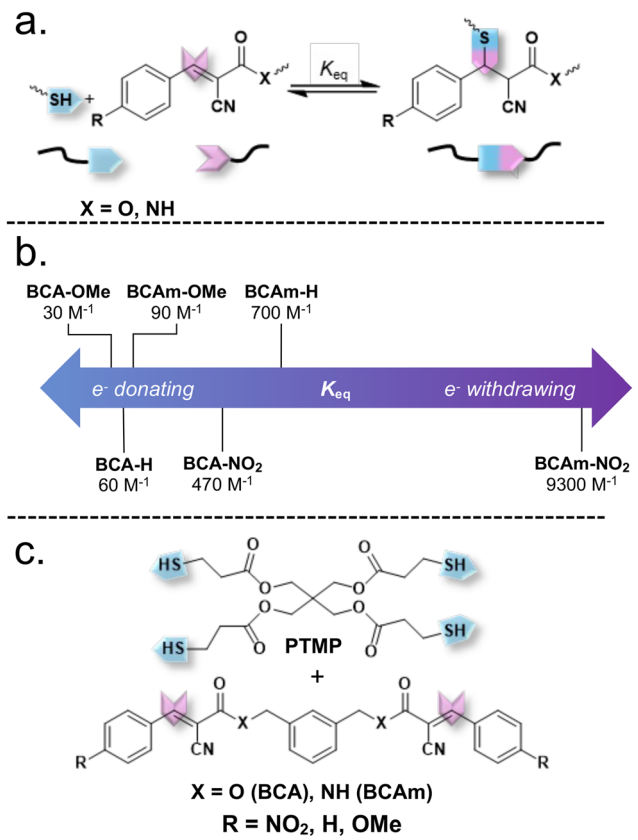

	BCA	BCAm
NO_2	1N	2N
H	1H	2H
OMe	1M	2M

Fig. 1 (a) General reaction scheme of the thia-Michael addition of a thiol to a benzalcyanoacetate (BCA) or benzalcyanoacetamide (BCAm) Michael acceptor. (b) Equilibrium constants (K_{eq}) of benzalcyanoacetate (BCA) and benzalcyanoacetamide (BCAm) Michael acceptors.[34–36] (c) Chemical structures of Michael acceptors and tetrathiol crosslinker pentaerythritol tetrakis(3-mercaptopropionate) (PTMP) studied in this work.

Prior work has shown that crosslinking ditopic BCA end-capped oligoethylene glycol acceptors with the tetrathiol crosslinker (PTMP) yields networks that are mechanically robust on account of a dynamic reaction-induced phase separation (DRIPS) process.[34] Interestingly, it was subsequently shown that tempering—defined as isothermally heating below a critical temperature followed by rapid quenching—of related thia-Michael networks gives access to a wide spectrum of mechanical properties from the same source material.[37,38] The tempering temperature (T_t) controls the amount of the thia-Michael bond formed in the network impacting the crosslink density and glass transition temperature (T_g). If the network is designed to have T_g around room temperature then materials with pluripotent-like properties can be accessed, in which, depending on the T_t, either stiff and brittle films (higher crosslink density and T_g above room temperature) or soft and extensible films (lower crosslink density and T_g below room temperature) can be prepared from the same source material.[37] Tempering at low temperatures results in a stiff material that could be used as a spoon, while tempering at higher temperatures yields a material that is a pressure sensitive adhesive. Furthermore, it has been shown that crosslinking BCA-based Michael acceptors with the PDMS-based polythiol afforded low T_g materials that exhibit both pressure-sensitive adhesive and hot-melt adhesive characteristics highlighting the inherent adhesive capability of these materials.[39]

Building on these insights, this work sought to explore if thia-Michael (tM) networks with T_g greater than room temperature could not only act as glassy adhesives but if tempering could be used to influence the strength of their adhesive bond. The majority of the previous studies on BCA/BCAm thia-Michael containing networks focused on polymer networks with T_g below or around room temperature,[34,37] thus it was of interest to explore the corresponding dynamic polymer glasses. To access higher T_g thia-Michael dynamic networks the core of the ditopic Michael acceptor was changed from the flexible oligoethylene glycol to a stiffer *meta*-substituted phenyl core (Fig. 1c). Expanding the library of materials further, both benzalcyanoacetate (X = O) and benzalcyanoacetamide (X = NH) Michael acceptors were synthesized allowing for an exploration of how the additional hydrogen bonding in the BCAm networks plays a role.

Results and discussion

Two classes of ditopic Michael acceptors based on either BCA and BCAm that bear three different *para*-substituted β-phenyl moieties (–NO_2, –H, –OMe; **1N**, **1H**, **1M**, **2N**, **2H**, and **2M**, respectively) were synthesized *via* a two-step procedure[34] (see SI for details). The appropriate bis-alcohol or bis-amine is reacted with 2-cyanoacetic acid or methyl 2-cyanoacetate to yield 1,3-phenylenebis(methylene) bis(2-cyanoacetate) or *N*,*N*′-(1,3-phenylenebis(methylene))bis(2-cyanoacetamide), respectively. The Michael acceptors **1R** and **2R** (where R denotes the *para* substitution on β-phenyl ring – *i.e.* NO_2, H or OMe) are

then prepared by reacting the bis(2-cyanoacetate) or bis(2-cyanoacetamide) with the appropriate *para*-substituted benzaldehyde *via* a Knoevenagel condensation (^{1}H and ^{13}C NMR Fig. S1–S12). The resulting acceptors **1R** or **2R** were mixed with the tetrathiol pentaerythritol tetrakis(2-mercaptoptopionate) (PTMP) in dimethylformamide (DMF) at a 1 : 1 stoichiometry of [thiol] : [double bond] to yield the thia-Michael (tM) networks **3R** or **4R**, respectively. Thermogravimetric analysis (TGA) confirmed that the resulting networks were solvent free (Fig. S13).

Differential scanning calorimetry (DSC) of the six materials reveals how the changes in the acceptor chemistry impacts their thermal transitions (Fig. 2a). Comparing the two different series, it is evident that the amide-containing **4R** materials exhibit higher T_g (as cast) than the ester-containing **3R** materials. This observation aligns with the presence of hydrogen bonding between amide groups in the **BCAm**-Michael acceptors within the **4R** material (Fig. S14 and S15). In both **BCA** and **BCAm** networks, T_g (as cast) was dependent upon the electronic nature of the R group on the β-phenyl ring, with more electron-withdrawing groups yielding higher T_g (as cast) values: BCAm series T_g (as cast) = 74 °C, 66 °C and 50 °C for **4N**, **4H**, **4M** respectively, and BCA series had T_g (as cast) = 61 °C, 7 °C and 5 °C for **3N**, **3H** and **3M** respectively (Table S1). This correlation of T_g (as cast) to electronic-withdrawing nature of Michael acceptors (and therefore higher K_{eq}s) was also observed in the previously studied PEG-based BCA networks,[34] and is consistent with a higher degree of crosslinking and reduced molecular chain mobility. Of the six materials only **3M** does not form mechanically robust films. The DSC of **3M** also showed a melting peak at 166 °C (Fig. 2a), which correlates with the melting of the starting Michael acceptor **1M** (T_m = 170 °C, Fig. S16), suggesting crystallization of the free Michael acceptor during film formation, which in turn hinders network formation. As such **3M** was not studied further. The other five materials show the presence of an upper transition (T_{UT}) in the DSC consistent with the previously studied BCA tM networks (Fig. 2a) that exhibit dynamic reaction-induced phase separation (DRIPS) during formation.[23] AFM imaging of these films confirmed DRIPS occurred in both **BCA** and **BCAm** networks, characterized by globular domains embedded in a continuous domain (Fig. 2b, S17 and S18).

The thermomechanical properties of the four glassy dynamic networks (**3N**, **4N**, **4H**, **4M**) probed using shear rheology showed a thermal transition corresponding to a T_g, consistent with the DSC (Fig. 2c, S19 to S22, see Fig. S23 for the data on **3H**). The glass transition temperatures (determined by the peak in tan δ) followed the same trend as the DSC thermograms; in which the **4R** films have higher T_g than the **3R** films and networks with more electron-withdrawing R groups have higher T_g. **4N** has the highest glass transition of 111 °C, followed by **4H** (76 °C), **4M** (66 °C), and **3N** (58 °C). The films that contain higher K_{eq} dynamic bonds, **4H**, **4N**, and **3N** display a distinct rubbery plateau modulus (1×10^6 Pa for **4N**, 2×10^5 Pa for **3N** and 5×10^4 Pa for **4H**) above T_g, while the storage modulus of **4M** continually decreased above T_g (Fig. 2c and

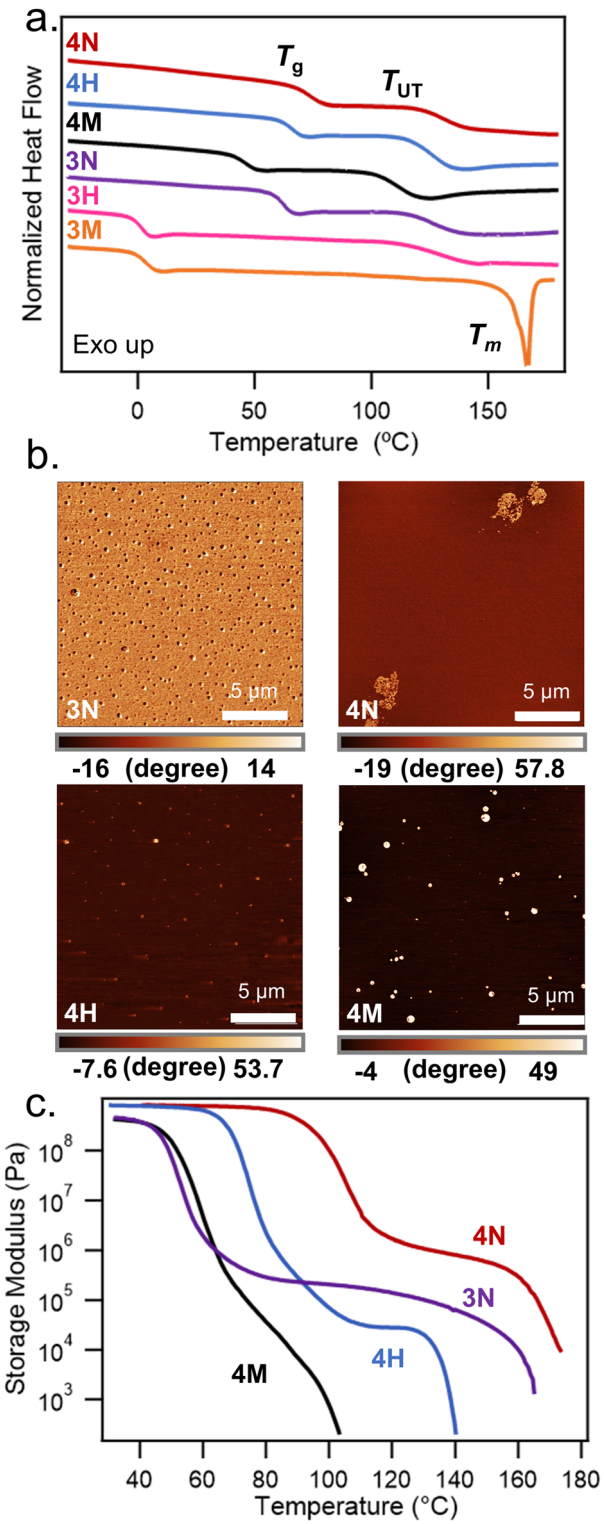

Fig. 2 (a) Differential scanning calorimetry (DSC) curves for **3N** (purple), **4N** (red), **4H** (blue), and **4M** (black). (b) Atomic force microscopy (AFM) phase images of **BCAm** and **BCA** networks showing dynamic reaction induced phase separation (DRIPS). Temperature of scans: **3N** (75 °C), **4N** (73 °C), **4H** (65 °C), **4M** (49 °C). Phase degrees are labeled below. (c) Shear rheology (temperature ramp rate 3 °C min^{-1}, frequency 1 Hz, parallel geometry) for **3N**, **4N**, **4H**, and **4M**.

S21). At higher temperatures a second thermal transition (T_{UT}) was observed, above which the materials entered the flow state as evidenced by a precipitous drop in modulus. For the dynamic material with the highest K_{eq} (**4N**) this second transition was observed at 153 °C, while **3N** and **4H** exhibit transitions at 138 °C and 127 °C, respectively. It is worthy of note that while the reaction of a thiol with **1N** and **2H** have similar K_{eq} values, the rheology of **3N** and **4H** is distinctly different, likely driven by the presence of the amide hydrogen bonding in **4H** as detected through Fourier-transform infrared spectroscopy (FTIR) at various temperatures (Fig. S14 and S15).

The next step was to explore if it was possible to temper these dynamic glasses. On account of their similarity in K_{eq} and thermal transitions **4H** and **3N** were selected as representative systems for probing differences in the physical properties of the **BCA-** *versus* **BCAm-**based materials. The tempering window of the tM networks was defined as the temperature range between T_g and T_{UT}; for **3N** and **4H**, this corresponds to *ca.* 70 to 110 °C based on their DSC curves. Shear rheometry measured the evolution of the storage modulus during tempering as a function of time in order to define the time required to reach equilibrium at each tempering temperature (T_t). Isothermal shear rheometry growth curves were taken for both **3N** and **4H** across a range of T_t. For both materials, storage modulus increased with tempering time and the required time to reach equilibrium shortened with increasing T_t. For **3N**, it took ~17 h at T_t = 70 °C for the storage modulus to plateau and ~15 min at T_t = 110 °C. For **4H**, it took ~21 h at T_t = 70 °C and ~35 min at T_t = 110 °C (Fig. S24). As can be seen, BCAm-based **4H** required longer tempering times compared to BCA-based **3N** at both tempering temperatures, which is presumably on account of the existence of amide hydrogen bonding present in **4H**. DSC of the tempered materials were then undertaken to explore if tempering impacts the materials thermal transitions. For **3N**, no significant changes in both T_g (tempered) and T_{UT} (tempered) are observed with different tempering temperatures (T_t = 70, 80, 90, 100 or 110 °C) (Table 1 and Fig. S25a, b). However, for **4H**, it was found that the T_g (tempered) after tempering had a strong correlation with tempering temperature (T_t) with T_g (tempered) decreasing from 84 °C (T_t = 70 °C) to 68 °C (T_t = 110 °C), while there was no significant difference in T_{UT} (Table 1 and Fig. S25a, b).

The relatively slow equilibration time of these materials opens the door to using tempering time (in addition to T_t) to control the material properties. When **3N** was tempered for different lengths of time at T_t = 70 °C or 110 °C, T_g remained unchanged (Fig. S25c and d). However, when **4H** is tempered at T_t = 70 °C there is a gradual increase in T_g (tempered) from 65 °C to 85 °C, reaching its equilibrium T_g (tempered) value in around 20 h (Fig. S25e). This timing is consistent with the equilibrium tempering time found through shear rheology (~21 h). The correlation between T_g (tempered) and tempering time demonstrates that material properties can not only be controlled using different T_t but also using different tempering time. At higher T_t (110 °C) there is no significant change of T_g (tempered) as a function of similar tempering times (Fig. S25f), which is also consistent with the shear rheology and suggests that the material reaches its equilibrium value in around 35 minutes. For consistency in the following studies, the tempering time for both **4H** and **3N** were set to 24 h for all tempering temperatures to ensure full equilibration.

Raman spectroscopy was used to probe changes in tM adduct fraction after tempering. For both **3N** and **4H**, spectra collected after tempering (T_t = 70 and 110 °C) at room temperature showed systematic shifts in the relative intensities of nitrile stretches corresponding to the Michael adducts (2253 cm^{-1} for **3N**, 2247 cm^{-1} for **4H**) and unreacted acceptors (2226 cm^{-1} and 2217 cm^{-1}, respectively) (Fig. 3a and S26). It was found in previous studies that the ratio of the integration of adduct peak to the integration of both peaks is proportional to the amount of tM adduct in the material.[37] The lower tempering temperature of 70 °C afforded an adduct peak fraction of 50% and 36% for **4H** and **3N**, respectively. Increasing the tempering temperature to 110 °C reduced the adduct peak fraction to 36% in **4H** and 21% in **3N**, reflecting a decrease in crosslink density (Fig. 3b). This reduction in crosslink density was manifested through a decrease in storage modulus observed *via* nanoindentation measurements performed at room temperature (Fig. 3c). Tempering at 110 °C results in a drop in the storage modulus (at 1 Hz) of **4H** to 2100 ± 121 MPa, from 3050 ± 148 MPa when tempered at 70 °C, while **3N** dropped to 1500 ± 125 MPa from 2040 ± 108 MPa over the same temperature range (Tables 1 and S2). Overall, **4H** exhibited higher storage moduli than **3N**, consistent with **4H** having higher crosslinking density (from Raman) as well as additional hydrogen bonding from the amide groups in **BCAm** acceptors, which are not present in the **BCA** acceptors.

To probe the effect of tempering on material properties and fracture toughness (K_c) of the dynamic glasses, nanoindentation of **4H** and **3N** films was carried out using a Berkovich indenter. Melt-pressed **4H** and **3N** films were tempered at 70 °C, 90 °C, and 110 °C, quenched on a cold (~0 °C) surface,

Table 1 T_g (tempered), T_{UT} (tempered), storage modulus, and fracture toughness of **3N** and **4H** tempered at various tempering temperatures (T_t)

	3N			**4H**		
T_t (°C)	70	90	110	70	90	110
T_g (tempered) (°C)	61 ± 1.1	62 ± 1.2	62 ± 0.9	84 ± 1.6	80 ± 1.4	68 ± 1.2
T_{UT} (tempered) (°C)	114 ± 1.8	115 ± 1.5	115 ± 1.6	112 ± 1.1	112 ± 0.7	111 ± 1.0
Storage modulus (MPa)	2040 ± 108	1680 ± 117	1500 ± 125	3050 ± 148	2600 ± 135	2100 ± 121
Fracture toughness (MPa $m^{1/2}$)	5.23 ± 0.4	4.66 ± 0.5	4.25 ± 0.4	7.25 ± 0.6	6.51 ± 0.5	5.28 ± 0.4

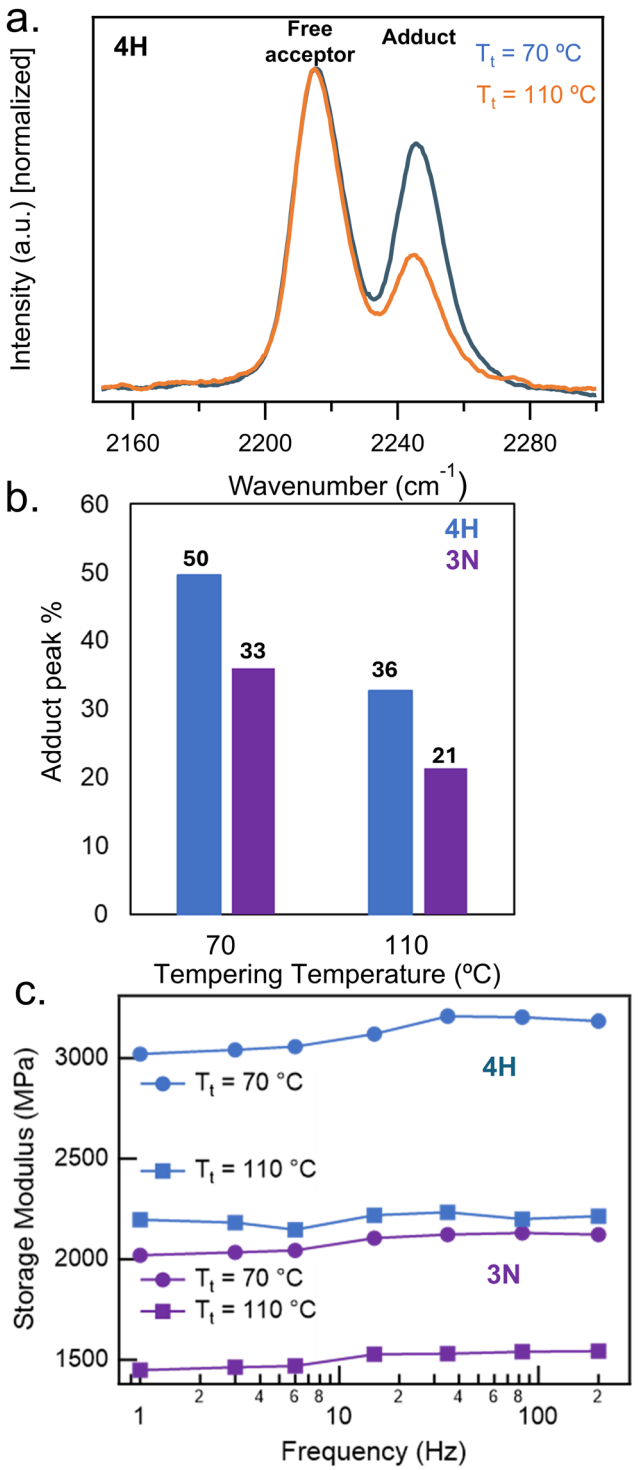

Fig. 3 (a) Room temperature partial Raman of **4H** films tempered at various temperatures, with the nitrile stretch of the free acceptor peak at 2217 cm^{-1} and the nitrile stretch of the tM adduct peak at 2247 cm^{-1}. (b) The % adduct of **4H** and **3N** films tempered at various temperatures (n = 5). (c) Room temperature frequency sweeps of **4H** and **3N** tempered at various temperatures, measured with a flat-punch tip.

and subsequently analyzed at room temperature by nanoindentation and AFM. Characteristic load–depth curves (Fig. S27) were used to derive values of hardness (H) and Young's modulus (E) as a function of tempering temperature. For **3N** when T_t is increased from 70 °C to 110 °C, there is a slight-to-no overall decrease (within experimental error) in both H and E (H: from 290 ± 62 MPa to 240 ± 35 MPa and E: from 4500 ± 390 MPa to 4000 ± 350 MPa). For **4N** a similar trend was observed with H exhibiting a slight decrease from 230 ± 57 MPa to 180 ± 38 MPa and the E showing a more significant decrease from 4400 ± 380 MPa to 2700 ± 340 MPa (Table S3). Decreasing tempering temperature does result in an overall increase in fracture toughness in both systems: **4H** tempered at 70 °C exhibited a 2 MPa $m^{1/2}$ increase relative to the film tempered at 110 °C: from 5.3 ± 0.4 MPa $m^{1/2}$ to 7.3 ± 0.6 MPa $m^{1/2}$, while the fracture toughness values of **3N** increased from 4.3 ± 0.4 MPa $m^{1/2}$ to 5.2 ± 0.4 MPa $m^{1/2}$ over the same tempering range (Fig. 4, Tables 1 and S3). At all tempering temperatures, **4H** was tougher than **3N**. Intermediate values obtained at tempering temperature of 90 °C (6.5 ± 0.5 MPa $m^{1/2}$ for **4H** and 4.7 ± 0.5 MPa $m^{1/2}$ for **3N**) confirmed that fracture toughness can be systematically tuned within this window by adjusting the tempering temperature. Additionally, aging tests were done with **3N** and **4H** samples where the fracture toughness of these films was measured every 24 h after tempering over a course of a week. Both samples were able to maintain their fracture toughness values and no significant decrease was observed (Fig. S29 and S30) in this time frame.

As mechanical differences were observed upon tempering these dynamic glasses it was of interest to explore if tempering would impact their adhesive properties. If the dynamic glass can be efficiently adhered to a given substrate and cohesive failure of the bond occurs, then it could be expected that these dynamic glasses would exhibit tunable adhesive behavior through tempering. To that end lap shear tests were conducted with **3N** and **4H** films tempered at 70 °C, 90 °C and 110 °C, using aluminum substrates at room temperature. Lap shear

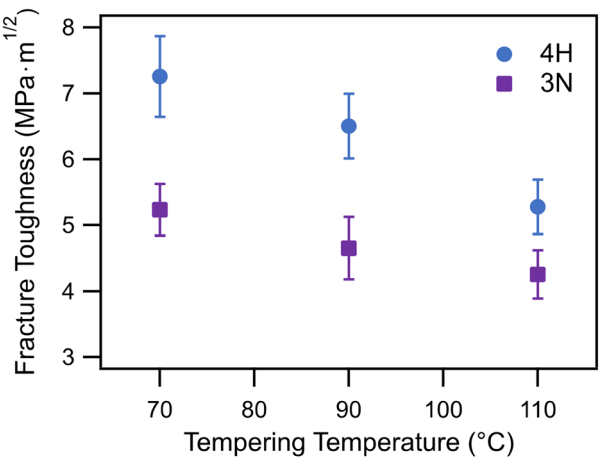

Fig. 4 Fracture toughness of **4H** and **3N** films tempered at various temperatures (n = 5).

samples were prepared with solvent-free melt-pressed **3N** and **4H** films, which were put in between two aluminum plates, clamped on the bonding site with two binder clips (exerting ~30 N pressure) and heated in the oven until the films became soft and attached onto the substrates. The bonding temperatures of **3N** and **4H** were chosen at the point when the material had softened enough (see Fig. 2c) to aid the bonding between the adhesive and substrates: **3N** at 150 °C and **4H** at 130 °C (if temperatures above 150 °C were used for bonding degradation was observed). Attempts to bond **4H** at the same temperature as **3N** (150 °C) resulted in the materials flowing out of the aluminum plates as the viscosity of this material is too low at this *T*. After bonding with the substrates, the lap shear samples were tempered at a given T_t for 24 hours, quenched in the fridge (~4 °C), and were tested under tension until adhesive bond failure at room temperature. As expected, results showed that the adhesive shear strength for both **3N** and **4H** samples were lowered with higher tempering temperatures, consistent with the tempering yielding a weaker dynamic glass. The aluminum plates bonded with **3N** had an adhesive shear strength (measured as maximum stress at break) of 4.9 ± 0.7 MPa at T_t = 70 °C and 2.7 ± 0.6 MPa at T_t = 110 °C while those bonded with **4H** recorded an adhesive shear strength of 5.9 ± 0.8 MPa at T_t = 70 °C and 3.6 ± 0.6 MPa at T_t = 110 °C (Table 2, Fig. 5a and S31). Across all conditions, **4H** exhibited higher shear strength than **3N** even with the fact that **4H** was bonded at a lower temperature, which was consistent with the previous mechanical characterization of the glasses. After the tests, both samples exhibited cohesive failure as demonstrated by the fact that sample was adhered to both sides of aluminum plates. Cohesive failure confirmed good surface adhesion between the samples and aluminum surfaces and that the interfacial bond strength was sufficiently high to result in bulk fracture of the dynamic network (Fig. 5c, left and S32). Rebonding tests were performed with both **3N** and **4H** samples, the samples were prepared and tested in the same way as previously described. After the test the substrates were reassembled at the same bonding site, clamped, and heated for 24 h. Both **3N** and **4H** went through three cycles of rebonding tests at T_t = 70 °C and were quenched to room temperature before testing. **4H** had consistent shear strengths, within error, over the three cycles. However, the adhesive shear strength of **3N** dropped from 4.9 ± 0.4 MPa to 4.0 ± 0.4 MPa after the first round of rebonding, and the shear strength slightly dropped to 3.8 ± 0.3 MPa after the second round (Fig. 5b). The reason for this difference in rebonding performance could arise from the rebonding process, where the modulus of **3N** at 150 °C is

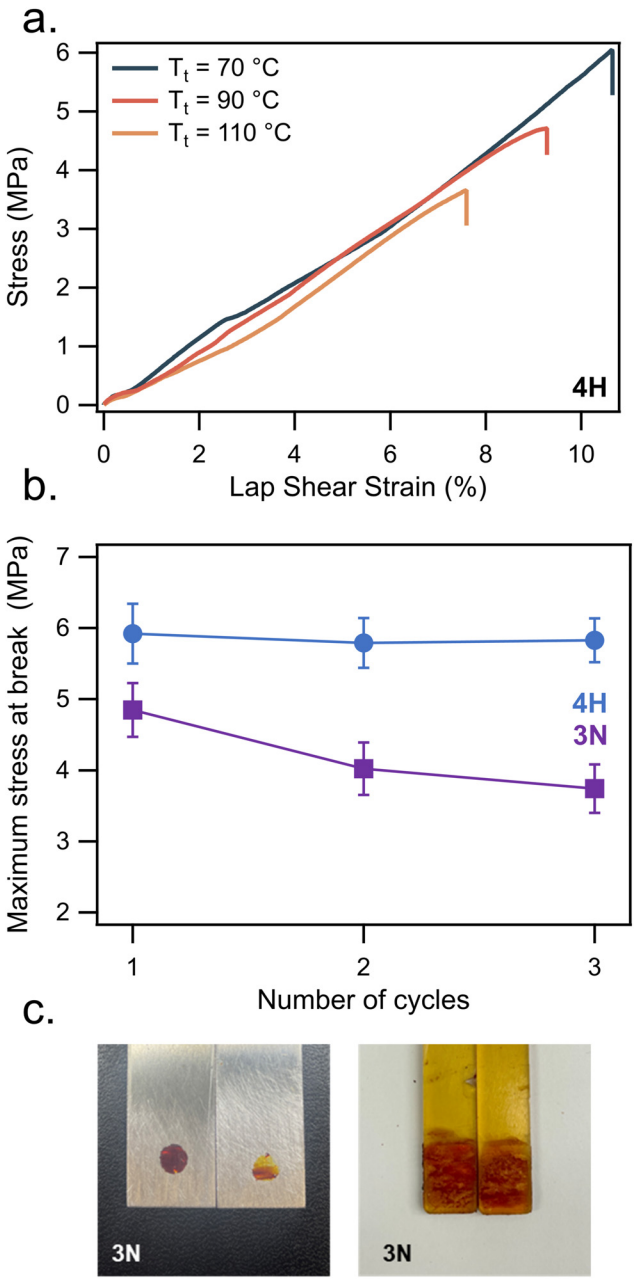

Fig. 5 (a) Representative room temperature stress–strain curves of the debonding of **4H** bonded to aluminum substrates after being tempered at various temperatures (*n* = 5). (b) Maximum stress at break at room temperature for rebonding tests of **3N** and **4H** with aluminum substrates (*n* = 3). (c) Representative photos of lap shear samples of **3N** after tests, showing cohesive failures with both substrates (left: aluminum, right: polyetherimide).

Table 2 Adhesive shear strength (measured as maximum stress at break) of **3N** and **4H** tempered at various tempering temperatures (T_t) (*n* = 5)

	3N			**4H**		
T_t (°C)	70	90	110	70	90	110
Adhesive shear strength (aluminum substrate) (MPa)	4.9 ± 0.7	3.3 ± 0.5	2.7 ± 0.6	5.9 ± 0.8	4.8 ± 0.6	3.6 ± 0.6
Adhesive shear strength (polyethermimide substrate) (MPa)	2.38 ± 0.3	1.89 ± 0.2	1.16 ± 0.2	1.92 ± 0.3	1.45 ± 0.2	0.95 ± 0.2

much higher than that of **4H** at 130 °C (see Fig. 2c) leading to less efficient bonding.

In addition to aluminum substrates, the adhesive capabilities of **3N** and **4H** were explored with polyetherimide substrates, chosen for their low surface energy and smooth, non-porous surfaces that can be challenging to form strong adhesive bonds. On account of the poor heat conductivity of polyetherimide substrates, samples prepared with melt-pressed films gave poor adhesion as the dynamic films did not soften/flow enough to adequately adhere to the substrate surface. Instead, lap shear samples were prepared using DMF plasticized films, which facilitated the bonding to the substrate by softening the adhesive and allowing it to better attach onto the substrate surface. The bonding process involved slowly heating the assembly that is held together with two binder clips clamped on both sides of the adhesive bonding site exerting ~30 N pressure. The residual DMF was then removed *via* vacuum oven drying. After solvent removal, lap shear samples were tempered at the designated temperatures (70 °C, 90 °C, and 110 °C) for 24 hours and were quenched to room temperature prior to testing. The resulting films were clear and bubble-free (Fig. S33); films were confirmed to have less than 1% DMF in weight as tested in TGA after the lap shear tests. As expected, the overall adhesion shear strength is less with these polyetherimide substrates than was observed in the above aluminum substrates. However, as with the aluminum substates, a clear trend was found in adhesive shear strength with T_t, with lower T_t's resulting in stronger adhesion (Fig. S34 and S35). **4H** had an adhesive shear strength of 1.0 ± 0.2 MPa at T_t = 110 °C and 1.9 ± 0.3 MPa at T_t = 70 °C while **3N** had an adhesive shear strength of 1.2 ± 0.2 MPa at T_t = 110 °C and 2.4 ± 0.3 MPa at T_t = 70 °C (Table 2). Different to what was observed with the aluminum substrate there is not a significant difference the adhesion capabilities of the two dynamic films to the polyetherimide substrates. This change in behavior could be related to differences in the surface adhesion of the two films to the lower surface energy substrates. While **3N** demonstrated cohesive failure (Fig. 5c, right), **4H** exhibited a mix-mode failure surface, suggesting the interface bond strength is on par with the bulk shear strength of **4H** (Fig. S36). For comparison, a commercial epoxy adhesive was tested on the same substrates at ambient temperature and displayed an adhesive shear strength of 1.73 ± 0.2 MPa but the bond failed adhesively, placing tempered tM networks on par with a commercial system while retaining cohesive failure.

Conclusions

In summary, this work developed thia-Michael dynamic polymeric glasses using ester-containing BCA- and amide-containing BCAm-based Michael acceptors. These materials exhibited a wide range of thermomechanical properties which were governed by the electronic nature of substituents on the acceptor. The glassy networks were shown to be temperable exhibiting significant changes to the material properties depending on the tempering temperature (T_t). Upon tempering at the upper and lower bounds of their tempering windows (70 °C and 110 °C), **3N** and **4H** demonstrated a 17% and 15% change in the adduct fraction within the networks. The change in adduct fraction, and therefore change in crosslinking density, manifested as a change in the thermomechanical properties of the glassy films. Comparison of the BCA film (**3N**) with the BCAm film (**4H**), which have similar K_{eq}s and thermal transitions, showed that the BCAm films take longer to reach equilibrium during tempering, consistent with the presence of additional hydrogen bonding in the amide-based networks. The longer time to reach equilibrium allows tempering time to be used to control the T_g of the BCAm glassy network. From a mechanical properties perspective tempering **4H** at 70 °C results in an increase in the storage modulus of *ca.* 940 MPa relative to the same film tempered at 110 °C, while **3N** increased *ca.* 540 MPa when tempered under the same conditions. In addition, the fracture toughness of **4H** and **3N** increased by 2.0 MPa $m^{1/2}$ and 1.0 MPa $m^{1/2}$, respectively, when comparing tempering at the upper and lower bounds of the tempering window. Moreover, these dynamic materials exhibited adhesion behavior and were shown to bond and rebond with aluminum substrates as well as bond lower surface energy polyetherimide substrates on par with commercial adhesives. Importantly, the level of adhesion of the networks to both substrates can be tuned by T_t consistent with the changes observed in the mechanical properties of the glassy networks, with higher T_t yielding lower adhesive shear strengths.

Conflicts of interest

There are no conflicts to declare.

Data availability

The data supporting this article have been included as part of the supplementary information (SI). Supplementary information is available. Data includes experimental procedures for the synthesis of the monomers and polymer network preparation as well as additional characterization of the compounds (TGA, FTIR, DSC, AFM, Rheology, Raman and lap shear tests) See DOI: https://doi.org/10.1039/d6py00373g.

Acknowledgements

This work was supported by the National Science Foundation under awards DMR-2104694 and DMR-2505198 and in part by the Army Research Laboratory under Cooperative Agreement Number W911NF-25-2-0156 and by the Army Research Office under agreement number W911NF-23-2-0075. NRB was supported by a NASA Space Technology Graduate Research Opportunity. The views and conclusions contained in this document are those of the authors and should not be interpreted as representing the official policies, either expressed or

implied, of the Army Research Laboratory, or the U.S. Government. The U.S. Government is authorized to reproduce and distribute reprints for Government purposes notwithstanding any copyright notation herein. This work made use of the shared facilities at the University of Chicago Materials Research Science and Engineering Center and the Soft Matter Characterization Facility, supported by National Science Foundation under award number DMR-2011854.

References

1 A. J. Kinloch, *Adhesion and Adhesives*, Springer Netherlands, Dordrecht, 1987.
2 J. S. Schlechte, *Advances in epoxy adhesives*, Elsevier, 2023.
3 A. Dong, Q. Liu, H. Yao, J. Ma, J. Cheng and J. Zhang, *ACS Appl. Mater. Interfaces*, 2025, **17**, 14578–14590.
4 W. Zhang, J. Wu, L. Gao, B. Zhang, J. Jiang and J. Hu, *Green Chem.*, 2021, **23**, 2763–2772.
5 Y. L. Tan, Y. J. Wong, N. W. X. Ong, Y. Leow, J. H. M. Wong, Y. J. Boo, R. Goh and X. J. Loh, *ACS Nano*, 2024, **18**, 24682–24704.
6 J. Hwang, D. Lim, G. Lee, Y. E. Kim, J. Park, M. J. Baek, H. S. Kim, K. H. Park, K. H. Ku and D. W. Lee, *Mater. Horiz.*, 2023, **10**, 2013–2023.
7 M. Gao, H. Wu, R. Plamthottam, Z. Xie, Y. Liu, J. Hu, S. Wu, L. Wu, X. He and Q. Pei, *Matter*, 2021, **4**, 1962–1974.
8 S. Zhang, H. Luo, S. Wang, Z. Chen, S. Nie, C. Liu and J. Song, *Int. J. Extreme Manuf.*, 2021, **3**, 035103.
9 H. Lee, D. S. Um, Y. Lee, S. Lim, H. J. Kim and H. Ko, *Adv. Mater.*, 2016, **28**, 7457–7465.
10 Z. Liu, Y. Tang, Y. Chen, Z. Lu and Z. Rui, *Chem. Eng. J.*, 2024, **497**, 154710.
11 P. Chakma and D. Konkolewicz, *Angew. Chem., Int. Ed.*, 2019, **58**, 9682–9695.
12 C. J. Kloxin, T. F. Scott, B. J. Adzima and C. N. Bowman, *Macromolecules*, 2010, **43**, 2643.
13 S. Samanta, S. Kim, T. Saito and A. P. Sokolov, *J. Phys. Chem. B*, 2021, **125**, 9389–9401.
14 B. Lewis, J. M. Dennis and K. R. Shull, *ACS Appl. Polym. Mater.*, 2023, **5**, 2583–2595.
15 D. Santiago, D. Guzmán, J. Padilla, P. Verdugo, S. De la Flor and À. Serra, *ACS Appl. Polym. Mater.*, 2023, **5**, 2006–2015.
16 Y. Xu, S. Dai, L. Bi, J. Jiang, H. Zhang and Y. Chen, *J. Agric. Food Chem.*, 2021, **69**, 9338–9349.
17 J. Wu, X. Yu, H. Zhang, J. Guo, J. Hu and M.-H. Li, *ACS Sustainable Chem. Eng.*, 2020, **8**, 6479–6487.
18 M. He, Y. Huang, J. Sun, Y. Dan, W. Zhao and L. Jiang, *React. Funct. Polym.*, 2022, **176**, 105283.
19 C. Y. Shi, Q. Zhang, B. S. Wang, M. Chen and D. H. Qu, *ACS Appl. Mater. Interfaces*, 2021, **13**, 44860–44867.
20 Y. Jin, Z. Wang, C. Hu, J. Wang, K. Yan, J. He, Z. Wang, Z. Wang and L. Yuan, *Green Chem.*, 2023, **25**, 1157–1168.
21 S. Pruksawan, S. Samitsu, Y. Fujii, N. Torikai and M. Naito, *Mater. Adv.*, 2020, **1**, 3182–3188.
22 C. Li, Y. Chen, Y. Zeng, Y. Wu, W. Liu and R. Qiu, *Eur. Polym. J.*, 2022, **162**, 110923.
23 Z. H. Zhao, P. C. Zhao, Y. Zhao, J. L. Zuo and C. H. Li, *Adv. Funct. Mater.*, 2022, **32**, 2201959.
24 X. Yang, M. Guo, Y. Wu, S. Xue, Z. Li, H. Zhou, A. T. Smith and L. Sun, *ACS Appl. Mater. Interfaces*, 2020, **12**, 56445–56453.
25 L. M. Sridhar, M. O. Oster, D. E. Herr, J. B. D. Gregg, J. A. Wilson and A. T. Slark, *Green Chem.*, 2020, **22**, 8669–8679.
26 S. Das, S. Samitsu, Y. Nakamura, Y. Yamauchi, D. Payra, K. Kato and M. Naito, *Polym. Chem.*, 2018, **9**, 5559–5565.
27 Y. Zhong, Y. Xu and E. V. Anslyn, *Eur. J. Org. Chem.*, 2013, **2013**, 5017–5021.
28 E. H. Krenske, R. C. Petter and K. N. Houk, *J. Org. Chem.*, 2016, **81**, 11726–11733.
29 C. E. Hoyle and C. N. Bowman, *Angew. Chem., Int. Ed.*, 2010, **49**, 1540–1573.
30 D. P. Nair, M. Podgórski, S. Chatani, T. Gong, W. Xi, C. R. Fenoli and C. N. Bowman, *Chem. Mater.*, 2013, **26**, 724–744.
31 D. Konkolewicz, A. Gray-Weale and S. Perrier, *J. Am. Chem. Soc.*, 2009, **131**, 18075–18077.
32 B. Zhang, Z. A. Digby, J. A. Flum, P. Chakma, J. M. Saul, J. L. Sparks and D. Konkolewicz, *Macromolecules*, 2016, **49**, 6871–6878.
33 V. Zhang, J. V. Accardo, I. Kevlishvili, E. F. Woods, S. J. Chapman, C. T. Eckdahl, C. L. Stern, H. J. Kulik and J. A. Kalow, *Chem*, 2023, **9**, 2298–2317.
34 K. M. Herbert, P. T. Getty, N. D. Dolinski, J. E. Hertzog, D. de Jong, J. H. Lettow, J. Romulus, J. W. Onorato, E. M. Foster and S. J. Rowan, *Chem. Sci.*, 2020, **11**, 5028–5036.
35 N. D. Dolinski, R. Tao, N. R. Boynton, A. P. Kotula, C. A. Lindberg, K. J. Petersen, A. M. Forster and S. J. Rowan, *ACS Macro Lett.*, 2024, 174–180.
36 G. L. Jackson, J. M. Dennis, N. D. Dolinski, M. Van Der Naald, H. Kim, C. Eom, S. J. Rowan and H. M. Jaeger, *Macromolecules*, 2022, **55**, 6453–6461.
37 N. R. Boynton, J. M. Dennis, N. D. Dolinski, C. A. Lindberg, A. P. Kotula, G. L. Grocke, S. L. Vivod, J. L. Lenhart, S. N. Patel and S. J. Rowan, *Science*, 2024, **383**, 545–551.
38 N. R. Boynton, C. M. Bennett, T. D. Hagan, G. R. Solymosy, C. A. Lindberg, N. A. Schaller, S. L. Vivod, S. N. Patel and S. J. Rowan, *ACS Macro Lett.*, 2025, **14**, 1728–1734.
39 K. M. Herbert, N. D. Dolinski, N. R. Boynton, J. G. Murphy, C. A. Lindberg, S. J. Sibener and S. J. Rowan, *ACS Appl. Mater. Interfaces*, 2021, **13**, 27471–27480.

